Electrostatic force spectroscopy of near surface localized states

View the article online for updates and enhancements.

Electrostatic force spectroscopy of near surface localized states

Aykutlu Dâna[1] **and Yoshihisa Yamamoto**[2]

[1] Advanced Research Labs, Department of Physics, Bilkent University, 06800 Ankara, Turkey
[2] Edward L Ginzton Laboratory, Stanford University, Stanford, CA 94305-4085, USA

E-mail: aykutlu@fen.bilkent.edu.tr

Abstract

Electrostatic force microscopy at cryogenic temperatures is used to probe the electrostatic interaction of a conductive atomic force microscopy tip and electronic charges trapped in localized states in an insulating layer on a semiconductor. Measurement of the frequency shift of the cantilever as a function of tip–sample bias voltage shows discrete peaks at certain voltages when the tip is located near trap centres. These discrete changes in frequency are attributed to one by one filling of individual electronic states when the quantized energies traverse the substrate conduction band Fermi energy as the tip–sample voltage is increased. Theoretical analysis of the experiment suggests that such a measurement of the cantilever frequency shift as a function of bias voltage can be interpreted as an AC force measurement, from which spectroscopic information about the location and energy of localized states can be deduced. Experimental results from the study of a sample with InAs quantum dots as trap centres are presented.

1. Introduction

As the semiconductor device size continues to shrink, new methods for characterization of electrical properties of materials and novel devices on the nanometre scale are required [1]. Detection of impurities, characterization of complex material stacks and interfacial properties, non-destructive electrical characterization of ultra-thin gate and capacitor dielectrics and 3D dopant profiling are a few of the challenges faced as the device size decreases to the nanometre scale. The challenge of electrical characterization of novel devices with smaller numbers of atoms motivates development of a technique that provides qualitative information about individual electronic states available within the devices.

Since its introduction [2], the atomic force microscope (AFM) and its spin-off techniques have been widely used in imaging and characterization of semiconductor surfaces. Electrostatic force based imaging techniques [3] such as Kelvin probe microscopy (KPM), scanning capacitance microscopy (SCM) and scanning spreading resistance microscopy (SSRM) among others have been used to electrically characterize surfaces. Still, an *in situ*, non-destructive technique for characterization of semiconductor surfaces and sub-surface

structures at the single electronic state level is greatly desirable. Because of its high force sensitivity, AFM has been used to detect the presence of individual electronic charges on the sample surface or inside layers near the surface as well as individual electron tunnelling events [4–7]. However, to be able to use the AFM to characterize individual states we still need to develop a method of obtaining information about the location, energy and dynamics of states on or near the semiconductor surface through force measurements. There has been significant work on this subject using force and frequency shift measurements to characterize localized states [8–10].

In this paper, to address this problem, we present a technique based on the measurement of electrostatic forces between a conducting AFM tip and charges localized at near-surface electronic states. A conducting AFM tip is used both as a gate electrode and as an electrometer that senses accumulated charge on the sample. Measurement of electrostatic forces between the tip and the sample as a function of the tip–sample bias voltage provide information about the location, energy and tunnelling dynamics of localized states. Regarding this measurement technique as a spectroscopy, we refer to it as electrostatic force spectroscopy (EFS) from here on. In the following sections, we begin by formulating the problem,

defining the sample structure to which this technique applies, give a theoretical analysis of the EFS experiment and provide experimental results.

2. Theoretical analysis of electrostatic force spectroscopy of localized states

When a biased conducting AFM tip is brought near a conducting sample surface, due to the finite tip–sample capacitance, charges of opposite sign accumulate in the tip and on the sample surface. This electrostatic interaction can be measured through deflection of the cantilever or through perturbation of its resonance frequency. If the sample is a semiconductor or a layered semiconductor/insulator structure with localized states, the electrostatic interaction between the tip and the sample deviates from a simple capacitor and the presence of localized states has to be accounted for in the analysis of the electrostatic forces. Based on a model of the sample, measurement of electrostatic interaction as a function of tip location and tip–sample bias voltage can provide data that can be inverted to give information about the location and energy of localized states or doping concentrations. Characterization of electronic states associated with traps inside thin dielectrics, states at semiconductor interfaces, states due to defects and the presence of adsorbates are important for the semiconductor technology. Therefore, we choose to restrict ourselves to a metal–insulator–semiconductor configuration with low density of localized states, as described in the following subsection.

2.1. Tip–sample configuration for an EFS experiment

The proposed sample configuration is schematically shown in figure 1(a). The conductive AFM tip is placed above an insulator-on-conductor structure, with a tip–sample separation of z_{ts}. In an actual experiment, the insulating layer can be a dielectric material deposited or grown on top of the highly conductive region, or a thin dielectric film otherwise placed on a flat conductive sample. In the analysis presented here, the sample is assumed to be a monolithic semiconductor where the conductive region and the insulating dielectric layer is defined by doping. The band diagram in such a configuration is illustrated in figure 1(b). The localized states can be due to impurities, dislocations, interface traps or intentionally introduced states due to the presence of quantum dots. The sample structure presented here has certain benefits. The localized states are inside an insulating layer so charge trapped in these states is not screened by free carriers. Also, since there is no doping in the top layer, the 3D potential profile generated by the tip is simple to analyse analytically. Moreover, the localized states can be charged and discharged by tunnelling of carriers from the bulk through the insulator. This modulation of the charge and resulting perturbation of the electrostatic force forms the basis of the proposed detection method.

2.2. Electrostatic model for calculating local potentials

Analysis of the EFS scheme begins with a model that describes the electrostatic force between the tip and sample and the potential profile inside the insulating layer. The electrostatic
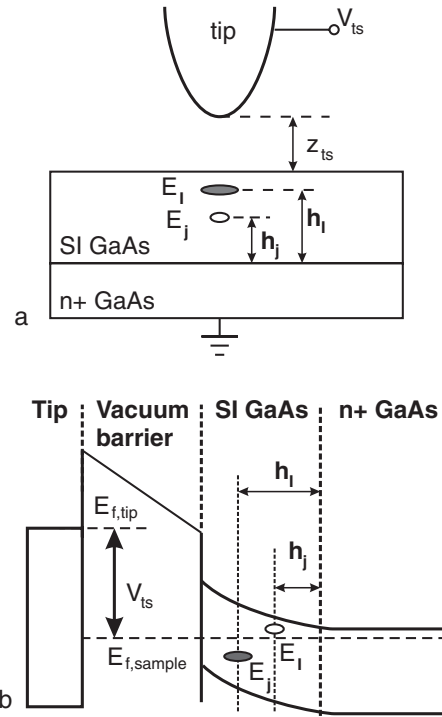

Figure 1. Schematic diagram of the EFS experiment. (a) Configuration of the tip and the sample that contains the states to be studied. States with energies E_i at heights h_i are located inside an insulating layer (semi-insulating GaAs) on top of a highly conductive ground plane (n⁺ GaAs). In the analysis and experiments presented in this work, the sample is chosen to be a monolithic semiconductor. The insulating and conducting regions are determined by doping. (b) Illustration of the energy band diagram. A filled state below the sample Fermi level $E_{f,sample}$ is shown with a filled ellipse. The states are dynamically charged and discharged by tunnelling of carriers from the n⁺ GaAs Fermi sea as the local potential is modulated.

problem described by the tip–sample system can be analysed analytically through a piecewise model of the tip. The charge density on the tip surface and the potential profile in the insulating region can be calculated approximately by modelling the tip as the union of a conic section and a spherical section as shown in figure 2. The overall tip–sample capacitance is assumed to be the sum of individual dihedral capacitances [11] formed by infinitesimal surface elements on the tip (shown as location (A) in figure 2) and corresponding surface elements on the surface (location (B) in figure 2).

The sphere–cone model of the tip can be used to estimate the local potential $V(x, z)$ (see figure 2) inside the insulating layer. The calculation of $V(x, z)$ can be done by noting that coordinate x is related to the geometrical model variable φ by a single-valued function $g(\varphi)$ as

$$x = g(\varphi) = r \sin \varphi + \frac{1 - \cos \varphi}{\sin \varphi}[z_{ts} + r(1 - \cos \varphi)]. \quad (1)$$

The local potential $V(x, z)$ is then given by

$$V(x, z) = \frac{V_{ts} z}{\epsilon_r} \left[\frac{\varphi[z_{ts} + r(1 - \cos \varphi)]}{\sin \varphi} + \frac{d_{ins}}{\epsilon_r} \right]^{-1} \quad (2)$$

where $\varphi = g^{-1}(x)$. Equation (2) agrees with a finite element analysis solution of the potential within 5% if $d_{ins}/\epsilon_r \ll z_{ts}$ and $r, z_{ts} \lesssim r$ and $|x| \lesssim 4r$.
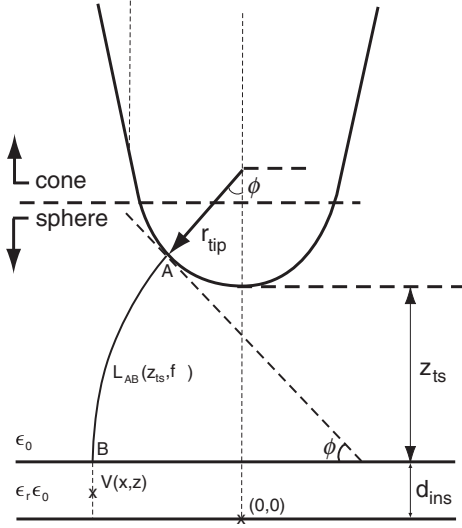
Figure 2. Description of the sphere–cone model of the tip–sample interaction. The AFM tip is modelled as the union of spherical and conical sections. The electrostatic problem is solved by integrating contributions of individual dihedral capacitors formed between surface elements on the tip (point (A)) and corresponding surface elements on the sample (point (B)). The tip–sample electrostatic force and potential profile $V(x, z)$ inside the dielectric can be accurately described by the model.

For a flat metal sample, the electrostatic force estimated through this model (sphere–cone model) can be expressed in terms of the tip length H_{tip}, tip radius r, tip–sample separation z_{ts}, and tip half-cone angle θ_0 as the sum of conical and spherical contributions

$$F_{\text{sc}} = F_{\text{sphere}} + F_{\text{cone}} \tag{3}$$

where the spherical and conical terms are given by

$$F_{\text{sphere}} = V_{\text{ts}}^2 \pi \epsilon_0 r^2 \frac{1 - \sin\theta_0}{z_{\text{ts}}[z_{\text{ts}} + r(1 - \sin\theta_0)]} \tag{4}$$

$$F_{\text{cone}} = \frac{V_{\text{ts}}^2 \pi \epsilon_0 \sin\theta_0{}^2}{(\pi/2 - \theta_0)^2} \left[\ln \frac{H_{\text{tip}}}{z_{\text{ts}} + r(1 - \sin\theta_0)} - 1 \right. $$
$$\left. + \frac{r \tan\theta_0}{z_{\text{ts}} + r(1 - \sin\theta_0)} \right]. \tag{5}$$

The validity of this model can be tested through measurements of force gradients of a biased tip as a function of the tip–sample separation. It is seen from the data presented in figure 3 that by fitting only the tip radius the model given in equation (3) predicts the tip–sample capacitance qualitatively with less than 5% error in the range $r/2 \lesssim z_{\text{ts}} \lesssim 4r$.

2.3. Model for charging of the localized states

For a given tip–sample geometry, and a given bias voltage V_{ts}, the energy of a localized state i, a distance x away from the tip axis and at a height h_i from the ground plane (see figures 1 and 2), is given by

$$E_i = E_{i,0} - eV(x, h_i) \tag{6}$$

where e is the electronic charge, $V(x, h_i)$ is given by equation (2) and $E_{i,0}$ is the energy of the state under zero bias.
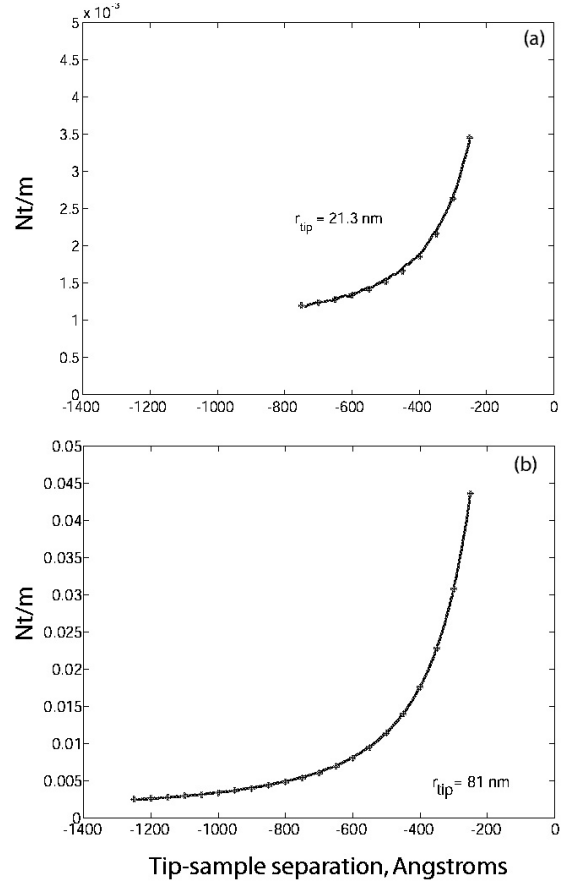

Figure 3. Electrostatic force gradient $\partial F_{\text{e}}/\partial z$ measured through frequency shift of the cantilever and theoretical estimation through equation (3) by fitting the tip radius. (a) A fresh tip has a fitted radius of $r = 21.3$ nm. (b) After contact imaging and deposition of metal on the surface through pulsing of the bias voltage, the tip radius increases to $r = 81$ nm.

For a given sample, if we define the dimensionless parameter $\alpha(x, z_{\text{ts}})$ as

$$\alpha(x, z_{\text{ts}}) = \frac{z + d_{\text{ins}}/\epsilon_r}{\varphi(z_{\text{ts}} + r(1 - \cos\varphi))/\sin\varphi + d_{\text{ins}}/\epsilon_r} \tag{7}$$

where φ is related to x through equation (1), we can rewrite equation (6) as

$$E_i = E_{i,0} - \frac{eV_{\text{ts}}h_i}{z_{\text{ts}}\epsilon_r + d_{\text{ins}}}\alpha(x, z_{\text{ts}}). \tag{8}$$

It worth noting that, for states on the tip axis, $\alpha(0, z_{\text{ts}}) = 1$ and equation (8) reduces to a simple voltage divider.

In thermal equilibrium, charge q_i of state i can be calculated through thermal statistics as

$$q_i = -\frac{e}{1 + \exp[(E_i - E_f)/k_B T]} \tag{9}$$

where $k_B T$ is the thermal energy.

When E_i is modulated in time, if the tunnelling time Γ_i^{-1} is finite but does not strongly depend on V_{ts}, the time dependent charge $\tilde{q}_i$ can be calculated through a first order differential equation as

$$\Gamma_i^{-1}\frac{d\tilde{q}_i}{dt} = -\tilde{q}_i + q_i(t). \tag{10}$$

Here $q_i(t)$ denotes q_i calculated through equation (9), and the time dependence is due to modulation of V_{ts} or z_{ts}. Γ_i stands for the tunnelling rate for state i for the given DC bias condition. The approximation presented in equation (10) would be valid only for a small signal modulation of the charge, since Γ_i depends exponentially on the potential barrier and cannot be assumed constant over a large modulation of the barrier. If a small signal sinusoidal modulation of V_{ts} or z_{ts} with frequency ω is present, $\tilde{q}_i$ will be given by a sinusoid that has a phase ϕ that depends on the modulation frequency and tunnelling rate Γ_i as

$$\phi = -\arctan(\omega/\Gamma_i). \qquad (11)$$

The modulated charge amplitude $\tilde{q}_i$ can be calculated through

$$\tilde{q}_i = \left\langle \frac{\partial q_i}{\partial V_{ts}} \right\rangle \tilde{V}_{ts} + \left\langle \frac{\partial q_i}{\partial z_{ts}} \right\rangle \tilde{z}_{ts} \qquad (12)$$

where the derivatives are calculated through equations (2), (6) and (9); averages denoted by brackets are taken over the modulation ranges of respective modulated variables. Here $\tilde{V}_{ts}$ and $\tilde{z}_{ts}$ are the modulation amplitudes of bias and tip–sample separation respectively. It is important to note that equation (12) refers to the AC modulated charge only. However, as the state falls below the Fermi level of the bulk, there is a DC shift in the charge, namely, the state goes from zero charge occupation to single charge occupation. This causes a DC frequency shift, as will be noted in the following section.

2.4. Electrostatic force model in the presence of localized states

The electrostatic interaction of the tip and the ground plane can be analysed accurately through the sphere–cone model. In the presence of localized states with charges q_i, there is additional contribution to the force from individual charges. For the sake of simplicity, the electrostatic force F_e that includes contributions from the localized charges and the background will be approximated by a parallel plate capacitor model given by [6]

$$F_e \cong \frac{\epsilon_r^2 \xi}{(\epsilon_r z_{ts} + d_{ins})^2} \left[\frac{\pi r^2 \epsilon_0 V_{ts}^2}{2} + \sum_i \frac{2 h_i q_i V_{ts}}{\epsilon_r} \right] \qquad (13)$$

where ξ is a geometric correction factor that can be calculated by equating F_e of equation (13) with all q_i being identically zero, to the electrostatic force of equation (3). In the parameter range $r/4 < z_{ts} < 2r$, ξ varies from 0.9 to 4.2 being equal to 1 if $z_{ts}/r = 0.4$. It is important to note that equation (13) is written assuming that the interaction is due to localized charges on the tip axis and a lumped charge due to tip–sample capacitance concentrated at the tip apex. In reality, force due to each localized state has to be corrected by integrating the force between q_i and the charge distribution on the tip. Also, extension of equation (13) to include the effect of charges away from the tip axis can be done by including the effect of geometry. The simplification made in derivation of the force in equation (13) assuming a lumped parallel plate capacitor model will only have an effect on the magnitude of the forces from individual charges.

2.5. Modulation of electrostatic force: localized state signatures

When an AC modulation of the tip–sample separation or tip–sample bias voltage is present, equation (13) can be used to estimate the AC modulated electrostatic force. Since the objective of the EFS experiment proposed in this work is to extract information about localized states through measurement of forces, in this subsection we will analyse the contribution from the localized states only. The AC force due to localized states can be calculated through

$$\tilde{F}_e = \sum_i \frac{\partial F_e}{\partial q_i} \tilde{q}_i \qquad (14)$$

where F_e and $\tilde{q}_i$ are given by equations (13) and (10) respectively. Equation (14) includes only the contribution due to modulation of the charges in the localized states and does not account for the modulated background force due to the presence of the bulk of the sample. The background contribution can be calculated by direct differentiation of equation (13) with respect to z_{ts} or V_{ts} with q_i set to zero. This background contribution will be analysed in the following subsections, since it proves to be a significant effect in the detection process.

Each term in the sum on the right-hand side of equation (14) contains information about the corresponding localized state, and we shall refer to it as the *signature* of that particular state. The signature force is a function of V_{ts}, the tip location with respect to the sample z_{ts}, the energy of the state $E_{i,0}$ and its height from the ground plane h_i. Therefore, measuring the modulated force for a set of values of V_{ts} and z_{ts} we can estimate $E_{i,0}$ and h_i.

When only a modulation of the bias voltage $\tilde{V}_{ts}$ is present, and the tip location is fixed, $\tilde{z}_{ts} = 0$, the signature for state i is

$$\tilde{F}_{e,i} = \frac{2 \epsilon_r h_i \xi V_{ts}}{(\epsilon_r z_{ts} + d_{ins})^2} \left\langle \frac{\partial q_i}{\partial V_{ts}} \right\rangle \tilde{V}_{ts}. \qquad (15)$$

Conversely, when only tip–sample separation is modulated and $\tilde{V}_{ts} = 0$, the signature is

$$\tilde{F}_{e,i} = \frac{2 \epsilon_r h_i \xi V_{ts}}{(\epsilon_r z_{ts} + d_{ins})^2} \left\langle \frac{\partial q_i}{\partial z_{ts}} \right\rangle \tilde{z}_{ts}. \qquad (16)$$

The dependence of the signatures in equations (15) and (16) on V_{ts} and z_{ts} is presented in figures 4 and 5, for a set of typical experimental parameters. It is seen from figure 4 that each state appears as a distinct peak when we plot $\tilde{F}_e$ against V_{ts}. This can be intuitively understood noting that, as the bias voltage is increased, the energy of the state traverses the Fermi energy of the ground plane and it is charged. Only when the state energy is close to the Fermi energy can the state charge be modulated by a modulation of the local potential. This modulation amplitude has the energy dependence of the derivative of the thermal distribution and thus the AC force amplitude appears as a peak when plotted versus V_{ts}. The signature voltage $V_{s,i}$ at which the force has peak amplitude is given through equation (8) for a state a distance x away from the tip axis as

$$V_{s,i} = \frac{E_{i,0}(\epsilon_r z_{ts} + d_{ins})}{e h_i \alpha(x, z_{ts})} \qquad (17)$$
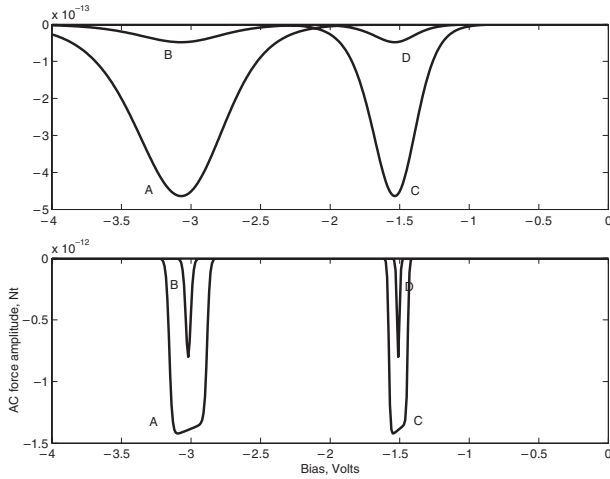
Figure 4. Theoretical force signatures of two states (top) under modulation of the tip–sample separation at $T = 77$ K. Curves (A) and (B) are calculated for a state with the parameters $E_{i,0} = 0.1$ eV, $h_i = 10$ nm, with modulation amplitude $\tilde{z}_{ts} = 1$ and 0.1 nm respectively. Curves (C) and (D) are for a state with the parameters $E_{i,0} = 0.1$ eV, $h_i = 20$ nm. Bottom, the same as the top except $T = 4$ K. The voltage at which the force peak occurs, and the width of the peak in terms of bias voltage, provide information about the energy and location of the state. The sample is chosen to be GaAs, with $\epsilon_r = 13.6$. The thickness of the insulating section is $d_{ins} = 30$ nm. The tip radius is $r = 20$ nm and $z_{ts} = 20$ nm. Negative amplitudes denote the fact that the modulated force has opposite phase to the modulation of the tip–sample separation.
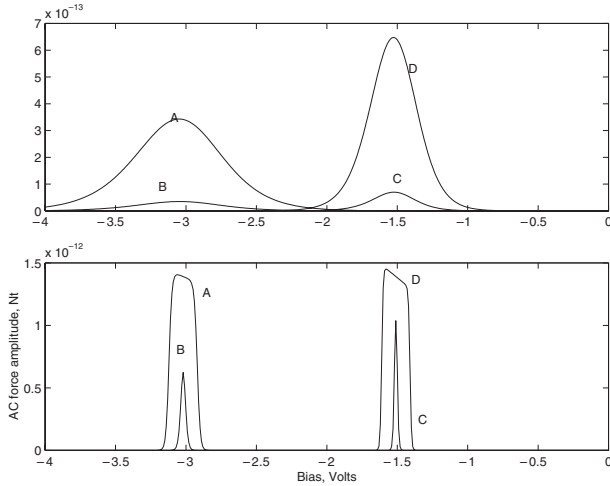

Figure 5. Theoretical force signatures of two states (top) under modulation of the bias voltage V_{ts} at $T = 77$ K. Curves (A) and (B) are calculated for a state with the parameters $E_{i,0} = 0.1$ eV, $h_i = 10$ nm, with modulation amplitude $\tilde{V}_{ts} = 10$ and 100 mV respectively. Curves (C) and (D) are for a state with the parameters $E_{i,0} = 0.1$ eV, $h_i = 20$ nm. Bottom, the same as the top except $T = 4$ K. Sample parameters are the same as in figure 4. Positive amplitudes denote the fact that the modulated force has the same phase as $\tilde{V}_{ts}$.

and in the limit of infinitesimal modulation amplitude the width $\Delta V_{s,i}$ of the peak in terms of bias voltage is

$$\Delta V_{s,i} = \frac{2k_B T (\epsilon_r z_{ts} + d_{ins})}{e h_i \alpha(x, z_{ts})}. \tag{18}$$

It is noted from figure 4 that, as the temperature is decreased and $k_B T$ becomes small compared to the modulation of E_i, the averaging of the derivative of q_i (denoted by the brackets in equations (15) and (16)) over the modulation range causes the signature to deviate from a Gaussian-like peak, and equation (18) no longer applies.

If $\Delta V_{s,i}$ can be measured accurately, then we can estimate $E_{i,0}$ from equations (17) and (18) as

$$E_{i,0} = \frac{2k_B T V_{s,i}}{\Delta V_{s,i}}. \tag{19}$$

To reduce the error in estimation of state parameters, one can repeat the EFS measurement changing only the tip location. From a set of EFS data taken at different values of the z_{ts}, it is possible to determine $V_{s,i}$, $\Delta V_{s,i}$ and $\partial V_{s,i}/\partial z_{ts}$. These parameters can then be used to solve for the three unknowns x, $E_{i,0}$ and h_i through equations (17), (18) and (19) uniquely.

In a case where measurement of $\Delta V_{s,i}$ has large error bounds due to imperfections of the measurement set-up, another method has to be devised to extract location, height and energy of the state. Due to the cylindrical symmetry of the tip, the potential of equation (2) will have circular equipotential contours. If the tip is scanned in the x–y plane keeping V_{ts} and z_{ts} constant, and $V_{s,i}$ is plotted as a function of x and y, the resulting image will exhibit circular patterns whose radii can be related to the experimental parameters and parameters of the state i using equation (17). The data resulting from such a measurement can also be used to estimate h_i as will be illustrated in the experimental sections.

Another important issue that has to be noted is the DC frequency shifts introduced by charging of individual states. As the charge of a state (equation (9)) is increased from zero to single electronic charge, the rightmost terms of the electrostatic interaction given by equation (13) cause a DC frequency shift. This is an extension to the signatures as calculated in equations (15) and (16). However, for our parameter range, this extension is about an order of magnitude smaller than the AC modulated charge signatures. This DC frequency shift effect gets less pronounced as the tip–sample separation is increased. Although this is a measurable effect, in the following sections, we ignore the DC frequency shifts due to individual charges and focus on the modulated charges.

2.6. Measurement of electrostatic forces: self-oscillation technique

The electrostatic force, modulated or DC, causes a deflection of the cantilever which can then be detected through a secondary detector, such as a laser interferometer. The minimum detectable electrostatic force is given by the thermomechanical noise limit, regardless of measurement frequency or technique. However, modulation frequency or measurement technique can be important in optimization of the signal-to-noise ratio (SNR), since a secondary detector cannot be assumed to be noiseless. For example, a typical laser interferometer used for cantilever deflection detection in our experiments has a noise floor of 2×10^{-3} Å Hz$^{-1/2}$. Referring to the figures 4 and 5, modulated electrostatic forces due to single states are on the order of 10^{-12} N for a typical experimental configuration. If a cantilever with a spring constant of say

$k_0 = 1$ N m^{-1} and quality factor $Q \sim 10^4$ is used, the peak deflection amplitude for a state signature will be on the order of 10^{-12} m if the modulation frequency is near DC and 10^{-8} m if the modulation frequency ω is on resonance with the cantilever mechanical resonance ω_0. The secondary detection limited charge sensitivity can be estimated to be 0.1 e (Hz)$^{-1/2}$ near DC and 10^{-5} e (Hz)$^{-1/2}$ on resonance. However, the thermomechanical noise floor for our cantilevers is 4×10^{-16} N Hz$^{-1/2}$ at 4 K independent of ω, and it corresponds to a fundamental limit for charge resolution of 4×10^{-4} e (Hz)$^{-1/2}$. Thermomechanical noise is dominant in the overall force measurement if $\omega \simeq \omega_0$.

Modulation frequency and technique is also important in realization of the EFS experiment. In order for the analysis presented for the modulation of V_{ts} to hold, z_{ts} must be kept constant, otherwise equation (15) will no longer describe the signature force correctly. In practice, this can be done by suppression of the cantilever oscillation by a feedback loop. However, modulation of the bias voltage with $\omega \simeq \omega_0$ requires tracking of the frequency shift of the cantilever due to the z-gradient of the background electrostatic force which is given by

$$\Delta\omega = -\frac{\omega_0 \xi \pi \epsilon_r^3 \epsilon_0 r^2 V_{ts}^2}{2k_0(\epsilon_r z_{ts} + d_{ins})^3} \qquad (20)$$

where k_0 is the spring constant of the cantilever.

The difficulties one has to overcome in order to realize the EFS experiment by modulating V_{ts} can be solved if z_{ts} is modulated instead of V_{ts}. Modulation of z_{ts} has two benefits: first, there is no need actively to suppress modulation of V_{ts} to validate assumptions made in analysis, since it can be biased by an external DC voltage source. Second, if the cantilever is oscillated by positive feedback or a phase-locked loop system on its resonance, the modulation of z_{ts} will automatically be always on resonance with the cantilever. These benefits motivate the use of self-oscillation of the cantilever.

A technical description of self-oscillation feedback can be found elsewhere [12, 13]. The self-oscillation technique was generally used to detect the force gradients due to time invariant interactions. This method can be applied to measurement of AC forces through frequency shift measurements. The method uses feedback to sustain the oscillation of the cantilever on its resonance, by measuring the AC deflection $\tilde{z}_{ts}$, phase shifting by $\pi/2$, conditioning it for amplitude control and feeding it back as a drive force $\tilde{F}_D$. The effect of the external feedback can be written by setting $\tilde{z}_{ts}(t) = \tilde{z}_{ts}\sin(\omega t)$ and $\tilde{F}_D(t) = \tilde{F}_D\cos(\omega t)$. When an external signal force $\tilde{F}_s(t) = \tilde{F}_s\sin(\omega t + \phi)$ is present, the oscillation amplitude $\tilde{z}_{ts}$ and oscillation frequency $\delta\omega$ can be calculated through

$$\tilde{z}_{ts} \cong \frac{Q}{k_0}(\tilde{F}_D + \tilde{F}_s\sin\phi) \qquad (21)$$

and

$$\delta\omega \cong \frac{\omega_0}{2k_0\tilde{z}_{ts}}\tilde{F}_s\cos\phi \qquad (22)$$

where Q is the quality factor of the cantilever. Approximations presented in equations (21) and (22) can be assumed valid if $\delta\omega \ll \omega_0$.

Inserting $\tilde{F}_s = \tilde{F}_{e,i}$ from equation (16), the signature of a state can be measured in the frequency shift of the cantilever
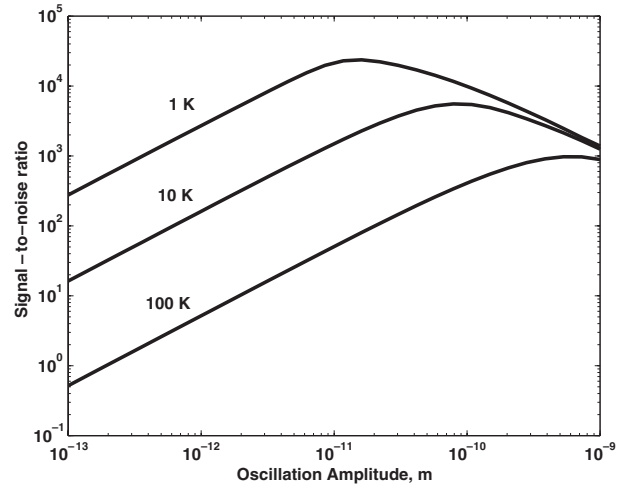
Figure 6. Signal-to-noise ratio for a single localized state in the frequency measurement technique as a function of temperature and oscillation amplitude $\tilde{z}_{ts}$. The state parameters are $E_{i,0} = 350$ meV, $h_i = 14$ nm. The total dielectric thickness is $d_{ins} = 30$ nm and $\epsilon_r = 13.6$. The cantilever resonance frequency is $\omega_0/2\pi = 73$ kHz, and the spring constant is $k_0 = 2.8$ N m^{-1}. The tip–sample separation is $z_{ts} = 12$ nm. The frequency detection is limited by the noise of the electronics at higher oscillation amplitudes. This fact causes the SNR to decrease if the oscillation amplitude is increased above an optimal value which is about 1 Å at 10 K.

in the self-oscillation configuration as

$$\delta\omega_i = \frac{\omega_0 \epsilon_r h_i \xi V_{ts}\cos\phi}{k_0(\epsilon_r z_{ts} + d_{ins})^2}\left\langle\frac{\partial q_i}{\partial z_{ts}}\right\rangle. \qquad (23)$$

The effect of temperature and oscillation amplitude on the overall SNR for this measurement scheme is illustrated in figure 6. The phase ϕ can be estimated by measuring $\tilde{z}_{ts}$ and $\delta\omega_i$ for a single state. The tunnelling rate Γ_i for the state can then be related to ϕ through equation (11).

In the self-oscillation method based measurement of the signatures, the total frequency shift is the sum of the background frequency shift of equation (20) and signature frequency shifts given by equation (23) as

$$\Delta\omega_{efs} = \Delta\omega + \sum_i \delta\omega_i. \qquad (24)$$

The minimum detectable charge in the frequency shift method is again given by the thermomechanical detection limit although the method of detection is through measurement of the frequency shift instead of deflection. Also, the presence of the self-oscillation feedback does not affect the value of the minimum detectable force. The only difference is that force noise translates to a fundamental frequency noise given by $\delta f = \sqrt{f_0 k_B T B / \pi k Q \langle a^2 \rangle}$ where f_0 is the cantilever resonance frequency, k_B is the Boltzmann constant, T is the temperature, k is the spring constant, Q is the quality factor and $\langle a^2 \rangle$ is the oscillation amplitude squared [12]. Note that this frequency noise can be obtained by inserting a thermomechanical force noise in place of $\tilde{F}_s$ in equation (22). The signal-to-noise ratio for an example state is shown in figure 6.

3. Experiment

The EFS experiments presented here use a home built low temperature AFM system that can operate down to 4.2 K. A fibre interferometer serves as the secondary detector. The laser wavelength is $\lambda = 1310$ nm, with 100 μW optical power incident on the cantilever, and the measured noise floor for deflection detection is 2×10^{-3} Å Hz$^{-1/2}$. Commercial Pt/Ir coated cantilevers with spring constants of $k_0 = 2.8$ N m^{-1} and resonant frequencies of $\omega_0 = 75$ kHz are used. Supplier specified tip lengths are $H_{tip} \simeq 10$ μm and the half-cone angle of the tip is 20°. The tip radius is not specified but can be extracted through force measurements to be $r \simeq 20$ nm. The quality factor of the cantilevers Q is around 150 in air and 15 000 at room temperature in vacuum, and ranges from 30 000 to 45 000 as the temperature is decreased from 77.3 to 4.2 K. Mechanical actuation of the cantilever oscillation using a piezoelectric element can produce spurious frequency shifts because mechanical structures can have multiple resonances near the operation frequency. Therefore, an electrostatic actuation scheme is used to oscillate the cantilever because of the constant phase and amplitude response in the frequency range of interest.

The sample is chosen to contain InAs QDs embedded in insulating GaAs since similar samples have been previously extensively studied for characterization of QD energy levels by optical and electrical methods [14, 15]. Based on previous capacitance spectroscopy experiments [16] incorporating similar InAs QDs, we expect the QD energies to be from 250 to 100 meV below the GaAs conduction band edge. It is also estimated that the number of confined energy levels and values of confined energies depend on QD size and up to 12 confined energy levels are estimated as the QD base diameter approaches 40 nm. Growth conditions have a strong effect on QD energy levels [14, 17] since gallium can replace indium in the dots and this alloying affects the QD bandgap. Although it is not possible to know the quantized energies of QDs only knowing the growth conditions, a rough estimation of the energy levels is still important for choosing the right experimental parameters of tip–sample separation and bias voltage range.

The sample is a molecular beam epitaxy (MBE) grown GaAs structure. First, a GaAs buffer layer with silicon doping of density 10^{18} cm^{-3} and thickness of 500 nm is grown, followed by an undoped GaAs layer of 15 nm thickness. Then a monolayer of InAs wetting layer was grown followed by a single layer of InAs QDs. The dots were capped by an undoped GaAs capping layer of 15 nm thickness. From a topographical AFM image of a test sample grown under the same conditions without a capping layer, the QDs were found to be about 20 nm in diameter and about 4 nm tall, with a surface density of 10^{10} cm^{-2}.

Contact mode topographic images of the surface were obtained prior to the EFS experiment to ensure the flatness and cleanliness of the surface. The force–distance curve with $V_{ts} = 0$ V provides information about the location of the surface, z_s. The drift of the scanner in x, y and z directions was characterized by repeating imaging and force–distance measurements with few-minute intervals, before and after the experiments. It was seen that when the AFM is operated at 4 K the drift is insignificant (~2 nm) over an hour and can be ignored.
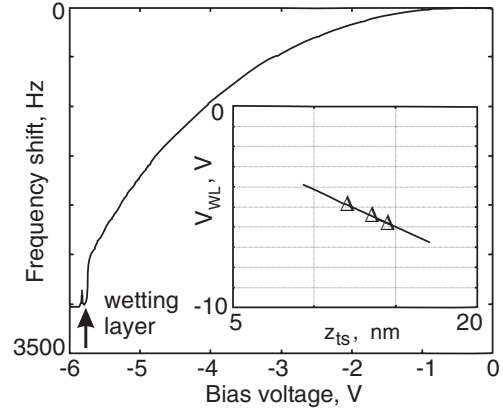

Figure 7. Observation of the InAs wetting layer (WL). The frequency shift due to background electrostatic forces follows a parabola which shows a sudden jump, an indication of the presence of a large number of states. The inset shows the theoretical estimation of the signature voltage V_{wl} as a function of z_{ts}. Fitting to the data, the state which causes the jumps is estimated to be $h_{wl} = 14$ nm above the ground plane and at an energy 25 meV below the GaAs conduction band.

3.1. Observation of the wetting layer

It is known from previous experiments [14] that the InAs wetting layer (WL) forms a two-dimensional electron gas (2DEG). In a crude approximation, it can be regarded as a collection of localized states and should present some form of signature in the EFS data. Study of the charging of the WL in our EFS experiment is interesting, since it produces a large signal due to the large number of electronic states. Also, the ground state energy of the WL with respect to the GaAs conduction band edge can provide a reference for the EFS data. Finally, the WL provides states at all locations on the sample and we do not have to find a proper location to observe the WL. It is known from optical and bulk capacitance spectroscopies that the presence of the WL states does not affect charge retention in individual InAs quantum dots. Therefore, WL does not limit us in measuring the quantum dot states. The bandgap of GaAs at room temperature is $E_{GaAs} = 1.52$ eV at 4.2 K, and surface pinning is assumed to be at the middle of the bandgap. In previous photoluminescence measurements of similar structures, the WL optical transition occurs at 1.42 eV. Therefore, if we assume for the sake of interpretation of the EFS data that WL is a localized state, the corresponding electron energy for that state under the zero-bias condition will be $E_{wl,0} = 330$ meV. The EFS data shown in figure 7 are collected with a tip–sample separation of $z_{ts} = 14.5$ nm, where z_{ts} is measured by a force–distance curve. A sudden change in the frequency shift indicates the presence of states that are charged when $V_{ts} = 5.83$ V. The EFS experiment is repeated at different tip–sample separations to fit the height h_{wl} and $E_{wl,0}$, and we find that $h_{wl} = 14$ nm, $E_{wl,0} = 360$ meV (shown in the inset of figure 7). The frequency shift jumps are not due to loop instabilities, because they occur at different absolute frequency shifts corresponding to different voltages. The repeatability of the WL peaks also provides evidence that this observation is not merely due to a loop instability. The discrepancy of the EFS results of $E_{wl,0} = 360$ meV from the optically obtained $E_{wl,0} = 330$ meV may be due to pinning of
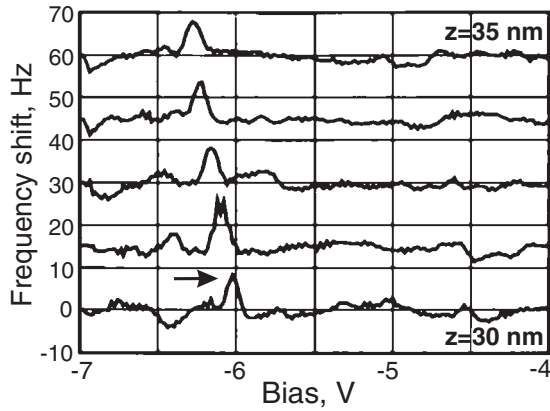
Figure 8. A single state signature can be isolated in the EFS data. The signature voltage $V_{s,i}$ moves to stronger biases as the tip–sample separation z_{ts} is increased from 30 to 35 nm. The large parabolic background is subtracted by high pass filtering and the curves are shifted for clarity. The vertical axis is the absolute value of the frequency shift. The fitted energy and location for this state are $E_{i,0} = 0.105$ eV, $h_i = 14$ nm, located $x = 51$ nm from the tip axis.

the GaAs surface at a slightly different energy than the middle of the bandgap, or due to the fact that any band-bending effects were ignored in our model.

3.2. Observation of localized states

In the EFS experiments performed with the aim of identifying QD energy levels, based on theoretical calculations and preliminary information given by the observation of the WL, choosing z_{ts} to be around 20 nm and $\tilde{z}_{ts}$ to be less than 1 nm, we expect to obtain an SNR greater than ten in a 100 Hz bandwidth for single states. In the capped sample, it is not possible to locate the dots through topographical imaging since the capping produces a flat surface. Therefore, EFS experiments were performed on a grid of points on a flat region of the sample.

Observation of isolated single signatures depends on the presence of isolated single states in the sample. If there are many states in the close vicinity of the tip, it is hard to distinguish individual peaks from a single EFS measurement.

A single isolated state signature from an EFS measurement is shown in figure 8. For this state, $V_{s,i}$ shifts towards negative voltages as z_{ts} moves from 30 to 35 nm. Since this signature is well isolated, it is possible to estimate the energy and depth of the state. Based on equations (17)–(19), we can estimate the state parameters to be $E_{i,0} = 0.105$ eV, $h_i = 14$ nm, located $x = 51$ nm from the tip axis.

Figure 9(a) is an example of EFS data with no signatures of localized states. Slowly varying background forces due to the presence of the ground plane were fitted and subtracted to clarify that there are no distinct peaks. Figure 9(b) shows EFS data for another location on the sample, with six distinct peaks in both frequency shift and oscillation amplitude. Similar signatures can also be observed near a QD in a sample grown exactly the same but without a capping layer (figure 9(c)). In the uncapped sample the signatures disappear when the tip is moved away from the QD, demonstrating that the signatures are indeed due to the QD. Energies can be fitted to each peak. The energies estimated from figures 9(b) and (c) and energies
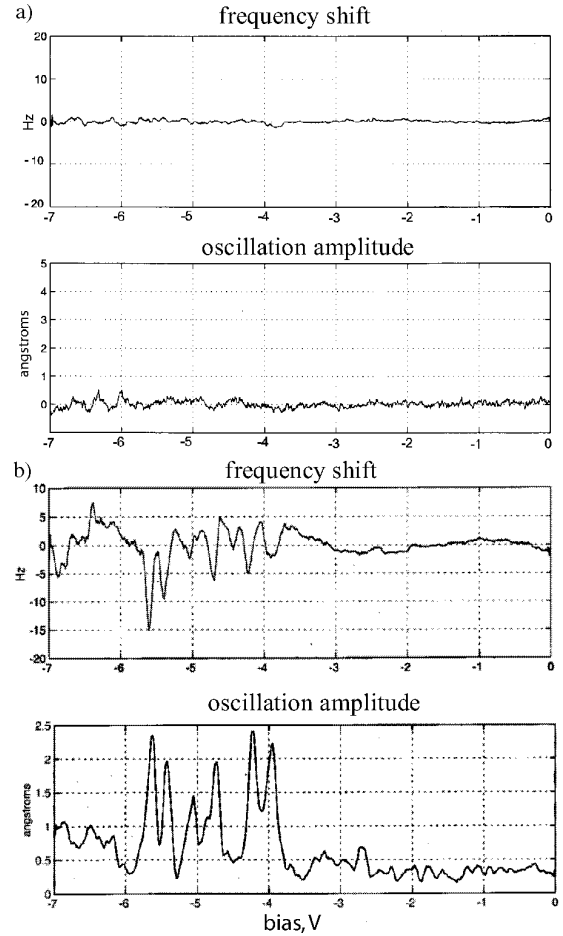

Figure 9. Observation of localized states. (a) Example of EFS data with no signatures, (b) on a site where there are localized states as evident from signatures. In the frequency shift data, the large parabolic background is subtracted for clarity by high pass filtering.

Table 1. Electron energy levels inferred from previous capacitive measurements for 20 nm base diameter capped dots, theory for 11.3 nm base diameter capped dots and this experiment involving 40 nm base diameter uncapped dot. Electron energies are shifted to match the ground state energies E_{s-1}.

Energy level (meV)	Theory	Capacitance data	EFS for capped QD
E_{s-1}	0	0	0
E_{s-2}		19	35
E_{p-1}	84	74	57
E_{p-2}		82	63
E_{p-3}	111	100	88
E_{p-4}		110	93

measured through conventional capacitance spectroscopy for similar dots in a previous measurements [15, 18] are compared in table 1 along with theoretical calculations by Wang *et al* [19]. The calculation by Wang *et al* does not take into account the Coulomb charging effects and estimates E_{s-1} to be 231 meV below the GaAs conduction band minimum.

To further illustrate the effect of tip location on $V_{s,i}$ one can plot the signature amplitude as a function of x and y in the vicinity of a localized state. Three signatures appear at a bias of -4.45 V (figure 10(e)), and as the voltage is increased to
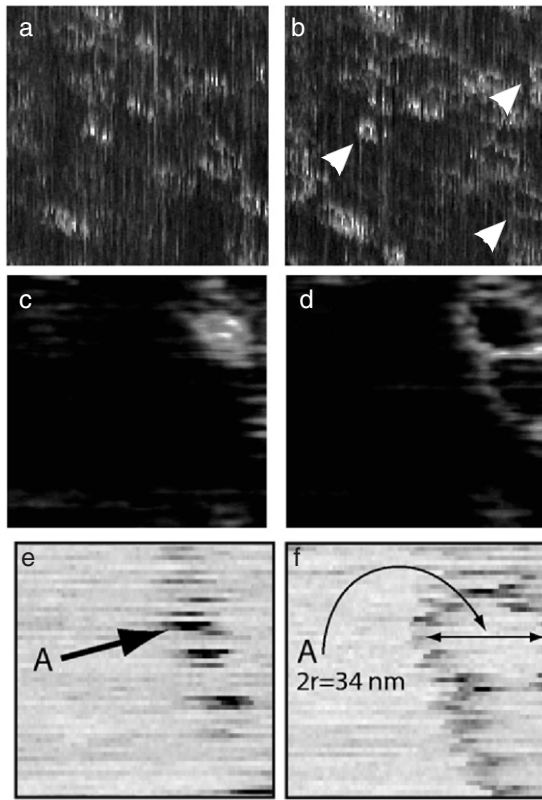
Figure 10. Constant height mode images taken over the sample with InAs quantum dots. The tip height is $z_{ts} = 20$ nm. (a) The bias voltage is $V_{ts} = -4.5$ V; a few bright spots and regions are visible. (b) At a stronger bias, $V_{ts} = -5.2$ V, a few spots are turned into circular shapes as shown by arrows (500 nm image size). (c) A close-up at $V_{ts} = -4.6$ V on one of the spots. (d) At $V_{ts} = -5.2$ V, the spots turn into two tangent circles (100 nm image size). (e) Signature amplitude plotted as a function of $x-y$ position of the tip in the vicinity of localized states. The tip height is $z_{ts} = 20$ nm and the bias voltage is $V_{ts} = -4.45$ V, (f) $V_{ts} = -5.15$ V. The signature located at point A first appears at $V_{ts} = -4.45$ V and has a radius of 17.3 nm at $V_{ts} = -5.15$ V. The theoretical estimate for the state from equation (17), $h_i = 14.5$ nm and $E_{i,0} = 205$ meV, correctly estimates the appearance and evolution of the signature (70 nm image size).

-5.15 V (figure 10(f)) the location of the signature peak defines a circular pattern, equivalent to an equipotential contour which is defined by equation (6). The energy and height of the state can be estimated as $h_i = 14.5$ nm and $E_{i,0} = 205$ meV by fitting equation (6) to the data.

4. Conclusions

A simplified theory of EFS generalized to a family of samples that has localized states inside a thin insulating layer is presented. The technique is capable of extracting information about individual localized states with a few-nanometre resolution and 4×10^{-4} electronic charge sensitivity. However, it must be noted that the presence of multiple states closely situated in position or energy complicates the inversion procedure. Application of the technique to InAs quantum dots embedded in a semi-insulating GaAs matrix is presented as a demonstration. The presented theory gives guidelines for the choice of cantilever and sample parameters for a given application of EFS. Potential applications include high resolution 3D dopant profiling in semiconductors, characterization of novel thin gate dielectrics and nondestructive characterization of self-assembled monolayer materials for nanoelectronic devices.

Acknowledgments

References

[1] 2001 *The International Technology Roadmap for Semiconductors–Metrology* (Austin, TX: Semiconductor Industry Assoc.)
[2] Binnig G, Quate C F and Gerber C 1986 *Phys. Rev. Lett.* **56** 930
[3] De Wolf P, Stephenson R, Trenkler T, Clarysse T, Hantschel T and Vandervorst W 2000 *J. Vac. Sci. Technol.* B **18** 361
[4] Schaadt D M, Yu E T, Sankar S and Berkowitz A E 1999 *Appl. Phys. Lett.* **74** 472
[5] Jones J T, Bridger P M, Marsh O J and McGill T C 1999 *Appl. Phys. Lett.* **75** 1326
[6] Klein L J and Williams C C 2001 *Appl. Phys. Lett.* **79** 1828
[7] Bussmann E, Kim D J and Williams C C 2004 *Appl. Phys. Lett.* **85** 2538
[8] Klein L J and Williams C C 2002 *Appl. Phys. Lett.* **81** 4589
[9] Luekede R and Cartier E 2001 *Appl. Phys. Lett.* **78** 3998
[10] Klein L J and Williams C C 2004 *J. Appl. Phys.* **95** 2547
[11] Hudlet S, Saint Jean M, Guthmann C and Berger J 1998 *Eur. Phys. J.* B **2** 5
[12] Albrecht T R, Grutter P, Horne D and Rugar D 1991 *J. Appl. Phys.* **69** 668
[13] Drig U, Steinauer H R and Blanc N 1997 *J. Appl. Phys.* **82** 3641
[14] Garca J M, Mankad T, Holtz P O, Wellman P J and Petroff P M 1998 *Appl. Phys. Lett.* **72** 3172
[15] Luyken R J, Lorke A, Govorov A O, Kotthaus J P, Medeiros-Ribeiro G and Petroff P M 1999 *Appl. Phys. Lett.* **74** 2486
[16] Medeiros-Ribeiro G, Pikus F G, Petroff P M and Efros A L 1997 *Phys. Rev.* B **55** 1568
[17] Hsu T M, Lan Y S, Chang W-H, Yeh N T and Chyi J-I 2000 *Appl. Phys. Lett.* **76** 691
[18] Medeiros-Ribeiro G, Garcia J M and Petroff P M 1997 *Phys. Rev.* B **56** 3609
[19] Wang L, Kim J and Zunger A 1999 *Phys. Rev.* B **59** 5768